

BrainCast: A Spatio-Temporal Forecasting Model for Whole-Brain fMRI Time Series Prediction

Yunlong Gao, Jinbo Yang, Li Xiao, Haiye Huo, Yang Ji, Hao Wang, Aiyong Zhang, and Yu-Ping Wang

Abstract—Functional magnetic resonance imaging (fMRI) enables noninvasive investigation of brain function, while short clinical scan durations, arising from human and non-human factors, usually lead to reduced data quality and limited statistical power for neuroimaging research. In this paper, we propose BrainCast, a novel spatio-temporal forecasting framework specifically tailored for whole-brain fMRI time series forecasting, to extend informative fMRI time series without additional data acquisition. It formulates fMRI time series forecasting as a multivariate time series prediction task and jointly models temporal dynamics within regions of interest (ROIs) and spatial interactions across ROIs. Specifically, BrainCast integrates a Spatial Interaction Awareness module to characterize inter-ROI dependencies via embedding every ROI time series as a token, a Temporal Feature Refinement module to capture intrinsic neural dynamics within each ROI by enhancing both low- and high-energy temporal components of fMRI time series at the ROI level, and a Spatio-temporal Pattern Alignment module to combine spatial and temporal representations for producing informative whole-brain features. Experimental results on resting-state and task fMRI datasets from the Human Connectome Project demonstrate the superiority of BrainCast over state-of-the-art time series forecasting baselines. Moreover, fMRI time series extended by BrainCast improve downstream cognitive ability prediction, highlighting the clinical and neuroscientific impact brought by whole-brain fMRI time series forecasting in scenarios with restricted scan durations.

Index Terms—Attention, fMRI, spatio-temporal modeling, time series forecasting

I. INTRODUCTION

Functional magnetic resonance imaging (fMRI), by measuring spontaneous fluctuations in blood oxygen level-dependent

This work was supported in part by the National Natural Science Foundation of China under Grants 62202442, 12261059, and 62401535, in part by the Natural Science Foundation of Jiangxi Province under Grant 20224BAB211001, in part by the Institute of Artificial Intelligence of Hefei Comprehensive National Science Center under Grants 23YGXT004 and Y1022502, in part by the NIH under Grants R01GM109068, R01MH104680, R01MH107354, R01EB006841, P20GM103472, and U19AG055373, and in part by the NSF under Grant 1539067.

Y. Gao and J. Yang are with the Institute of Advanced Technology, University of Science and Technology of China, Hefei 230052, China.

L. Xiao and Y. Ji are with the MoE Key Laboratory of Brain-Inspired Intelligence Perception and Cognition, University of Science and Technology of China, Hefei 230052, China (e-mail: xiaoli11@ustc.edu.cn).

H. Huo is with the School of Mathematics and Computer Sciences, Nanchang University, Nanchang 330031, China.

H. Wang is with the MoE Key Laboratory of Brain-Inspired Intelligence Perception and Cognition, University of Science and Technology of China, Hefei 230052, and also with the Anhui Province Key Laboratory of Biomedical Imaging and Intelligent Processing, HFCNS Institute of Artificial Intelligence, Hefei 230088, China.

A. Zhang is with the School of Data Science, University of Virginia, Charlottesville, VA 22903, USA.

Y.-P. Wang is with the Department of Biomedical Engineering, Tulane University, New Orleans, LA 70118, USA.

(BOLD) signals, has emerged as a preferred tool for functional imaging in noninvasive neuroscience studies [1], [2]. It enables the characterization of brain activity and large-scale functional connectivity, providing critical insights into both normal cognition and neurological disorders [3], [4]. Despite its broad applications, a persistent challenge in clinical settings is that fMRI scan durations are often short, due to participant-related factors (e.g., reduced tolerance for long-duration scans in psychiatric, pregnant, or younger and elder participants) and practical constraints (e.g., scan cost or protocol limitations) [5], [6]. Short-duration scans typically result in lower-quality fMRI data, characterized by reduced signal-to-noise ratio, compromised test-retest reliability, and diminished sensitivity in downstream analyses [7]–[9]. Although extending fMRI scan duration can alleviate these issues, longer acquisitions will increase participant burden and also the susceptibility to motion artifacts, and thus are not generally feasible in routine clinical practice [10]. Recent evidence further suggests that longer scans increase statistical power and cost-efficiency in whole-brain association studies [11]. These observations collectively motivate the development of methodology based approaches that can effectively extend fMRI time series without additional data acquisition.

Beyond data augmentation, the ability to predict future brain activity from historical fMRI data offers a complementary and potentially powerful means of understanding neural dynamics. On the other hand, accurate fMRI time series forecasting may facilitate the study of intrinsic brain process, enhance the modeling of interregional interactions, and enable applications such as cognitive assessment, disease phenotyping, and brain-computer interface. From a signal analysis perspective, fMRI time series exhibit strong temporal correlation and structured fluctuations, indicating that future fMRI data is partially predictable from previous observations [12], [13]. However, to the best of our knowledge, few methods have been specifically developed for fMRI time series forecasting.

Recent advances in deep learning have led to substantial progresses in generic time series forecasting, particularly in capturing complicated temporal dependencies. For instance, recurrent neural network (RNN) and long short-term memory (LSTM) models can model short-term temporal dependencies [14], [15], while Transformer-based architectures leverage attention mechanisms to learn long-range temporal dependencies [16]–[18]. These models have demonstrated notable success in time series prediction across domains such as traffic flow and power consumption. Nevertheless, they are not tailored for fMRI time series forecasting, in which fMRI time series are characterized by considerable noise, nonstationary dynamics, and rich inter-regional dependencies. For such data, forecasting performance

relies not only on temporal modeling within individual regions but also on considering interactions across brain regions.

In [19], BrainLM was built on a masked autoencoder framework for large-scale self-supervised pretraining, treating future fMRI time series prediction as an auxiliary task without explicitly modeling inter-region interactions. Generative Adversarial Networks (GANs) have been investigated for fMRI time series forecasting, but were restricted to low-frequency components from a single region within the default mode network (DMN), instead of whole-brain data [20]. Although more recent studies have attempted to account for spatio-temporal dependencies in fMRI data by graph neural network (GNN)- and Transformer-based models [21]–[23], their focus has primarily been on advanced representation learning for brain functional connectivity analyses, rather than explicit fMRI time series forecasting. As a result, whole-brain fMRI time series forecasting remains insufficiently explored, highlighting the need for joint coordination of temporal dynamics and spatial interactions.

In this paper, we address this gap via proposing BrainCast, a spatio-temporal forecasting framework specifically designed for whole-brain fMRI time series forecasting. As illustrated in Fig. 1, BrainCast utilizes a sliding-window partition strategy to formulate forecasting tasks and integrates spatial and temporal information in a unified architecture that forecasts whole-brain fMRI time series over a future horizon, given prior fMRI time series from a predefined look-back. BrainCast consists of three main modules: i) a Spatial Interaction Awareness (SIA) module used to explicitly characterize inter-region-of-interest (inter-ROI) interactions by embedding each ROI (variate) time series as a token; ii) a Temporal Feature Refinement (TFR) module introduced to enhance both low- and high-energy temporal components for capturing intrinsic neural dynamics within every ROI; and iii) a Spatio-temporal Pattern Alignment (SPA) module designed to align spatial and temporal representations from SIA and TFR, respectively, for producing informative whole-brain features, followed by a prediction head that forecasts the target fMRI time series. In addition, extensive experiments on resting-state and task fMRI datasets from the Human Connectome Project (HCP) [24] demonstrate the superiority of BrainCast over state-of-the-art time series forecasting baselines. Furthermore, extending fMRI time series using BrainCast results in more accurate cognitive ability prediction, underscoring the broader potential of fMRI time series forecasting for neuroscience research and clinical applications.

The contributions of this paper can be summarized below.

- This paper is among the first to examine fMRI time series forecasting as a multivariate time series prediction problem and to jointly model inter-ROI spatial interactions and intra-ROI temporal dynamics in a unified architecture.
- We propose BrainCast tailored for whole-brain fMRI time series forecasting, which incorporates SIA, TFR, and SPA modules to account for inter-ROI dependencies, nonstationary temporal dynamics, and heterogeneous spatio-temporal representations, respectively, for improved forecasting accuracy.
- Experimental results on large-scale fMRI datasets demonstrate that BrainCast outperforms several competitive time series forecasting models across multiple evaluation met-

rics. In addition, we show that fMRI time series extended using BrainCast lead to improved cognitive ability prediction, providing empirical evidence that whole-brain fMRI forecasting can enhance brain–cognition analyses, particularly under limited fMRI scan durations.

The remainder of this paper is organized as follows. Section II reviews related studies on time series forecasting and brain fMRI signal analysis. Section III presents the proposed BrainCast framework in detail. Section IV reports experimental results on fMRI datasets from the HCP, followed by discussions on visualization, hyperparameter influence, and applications in cognitive ability prediction in Section V. Section VI concludes this paper.

II. RELATED WORK

A. Time Series Forecasting

Deep learning models have demonstrated great potential in time series forecasting. For example, RNN-based models, such as RNNs and LSTMs [14], [15], have been presented through the extraction of temporal information from historical data for predicting future data, yet they are ordinarily limited in capturing long-term dependencies within time series. To address this issue, recent studies have begun to explore alternative architectures, e.g., Temporal Convolutional Network and Transformer [16], [25]. Particularly, the self-attention mechanism in Transformer enables effective modeling of long-range dependencies. Early Transformer-based models [26], [27] treated all variables at the same time point as one single token, which often led to semantic entanglement among variables and suboptimal performance. To mitigate this, PatchTST [28] presented a channel-independent approach that processed every variable separately. While this process improves clarity in variable representations, it incurs increased training time and fails to model interactions between variables. In [29], iTransformer was proposed to overcome these limitations by regarding each complete time series as a token, which allows the model to effectively capture inter-variable relationships. In parallel, GNN-based models have proven well suited in exploiting coupled temporal and spatial dependencies [30], [31]. Collectively, these advances have led to significant progress in time series forecasting and/or analyses. However, the majority of these above models were introduced for domains such as traffic flow and electricity usage, and are not specifically tailored to fMRI data. By contrast, fMRI time series exhibit different traits, e.g., substantial noise, nonstationary dynamics, and complicated inter-ROI interactions, which pose unique challenges for time series forecasting that are not adequately accounted for by existing forecasting models.

B. Brain fMRI Data Analysis

In recent years, significant advances have been made in the application of fMRI analysis techniques. Convolutional Neural Networks (CNNs) were among the earliest deep learning models applied to the analysis of diverse neurological disorders and brain connectivity patterns, such as BrainNetCNN and Convolutional Auto-Encoder [32]–[35], and have demonstrated encouraging performance. In addition, GNNs have displayed strong potential in brain connectivity network analysis owing to their

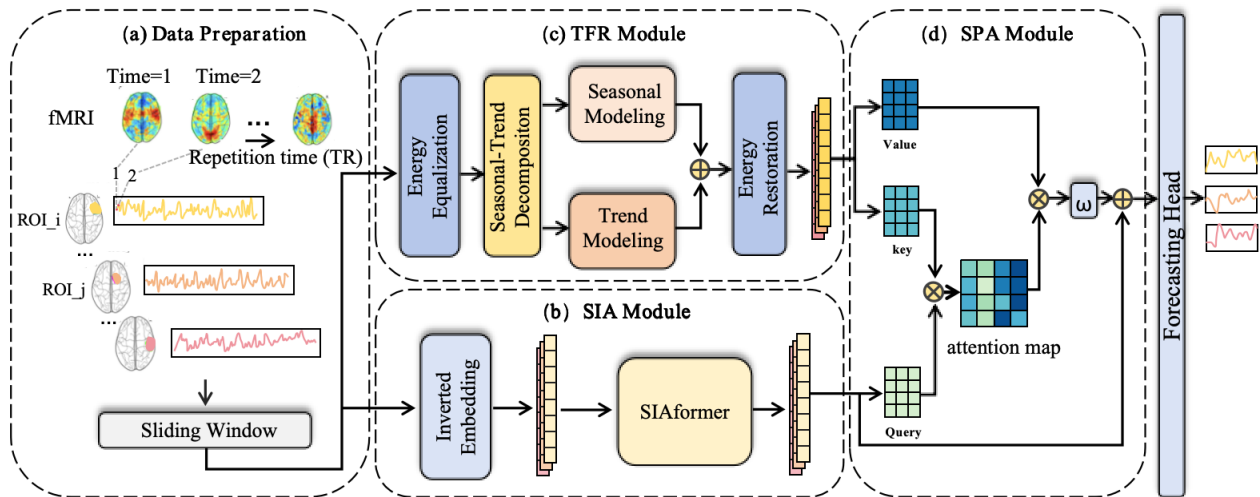


Fig. 1: The overall framework of BrainCast. (a) fMRI data preprocessing; (b) The Spatial Interaction Awareness (SIA) module for learning between-ROI spatial interactions; (c) The Temporal Feature Refinement (TFR) module for extracting temporal dynamics within every ROI; and (d) The Spatio-temporal Pattern Alignment (SPA) module for aligning spatio-temporal representations across ROIs and time points.

powerful capability to capture local structural information between ROIs [36]–[38]. For instance, BrainGNN adopted graph convolutional layers to enable biomarker prediction at both the population and individual levels [39]. Dynamic GNNs further exploited the dynamics of brain connectivity to consider time-varying interactions between ROIs [40]. More recently, Transformer-based models have attracted increasing attention owing to their superior ability to learn long-range dependencies [41], [42], and have been successfully applied in fMRI data analysis [43]. Although the above mentioned models have significantly advanced fMRI data analysis, most existing studies remain focus on characterizing observed fMRI data, with limited attention to modeling and forecasting future whole-brain fMRI time series. Remarkably, BrainLM leveraged a masked autoencoder architecture to pre-train a self-supervised model on large-scale fMRI datasets [19], where future fMRI time series forecasting served as an auxiliary task and inter-ROI interactions were not explicitly emphasized. In [20], a GAN-based model was developed for forecasting future fMRI time series; however, the forecasting was restricted to low-frequency components of fMRI time series from one single ROI within the DMN, rather than whole-brain fMRI time series.

III. METHODS

A. Problem Definition

Given fMRI data of a subject, it is a multivariate time series with N variables, in which the N variables correspond to the pre-defined N ROIs, and the i -th univariate time series is the observed fMRI responses of the i -th ROI over a period of run duration for $1 \leq i \leq N$. We apply a sliding window partition technique on the fMRI data to generate sequential samples, as illustrated in Fig. 2, where the window size is set to $L+T$, the stride is set to s , and the fMRI time series over every sliding window is referred to as a sample. For each sample, let the first L -point fMRI time series $\mathbf{X}_P = [x_1, x_2, \dots, x_L] \in \mathbb{R}^{N \times L}$ be

the previous data, and the following T -point fMRI time series $\mathbf{X}_F = [x_{L+1}, x_{L+2}, \dots, x_{L+T}] \in \mathbb{R}^{N \times T}$ be the future data, where $x_i \in \mathbb{R}^N$ represents the observed fMRI responses of all ROIs at the i -th time point. The fMRI time series forecasting task we study in this paper is to establish a mapping from the previous data \mathbf{X}_P to the future data \mathbf{X}_F .

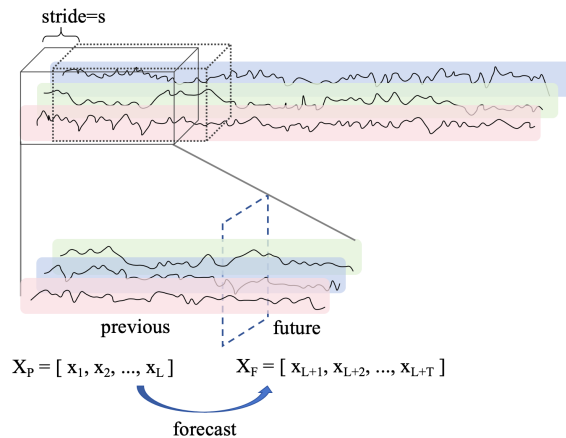


Fig. 2: A sliding window partition technique on the fMRI data to generate sequential samples.

To do so, we propose BrainCast, a spatio-temporal forecasting model for brain fMRI time series prediction. As shown in Fig. 1, BrainCast includes three important components, i.e., a Spatial Interaction Awareness (SIA) module formulated to uncover direct spatial interactions between distinct ROIs; a Temporal Feature Refinement (TFR) module tailored to capture the intrinsic temporal dynamics within every ROI; and a Spatio-temporal Pattern Alignment (SPA) module leveraged to align heterogeneous spatial and temporal features for robust whole-brain representations. Benefiting from this architecture, BrainCast enables accurate, reliable prediction of multi-region fMRI time series. The details of the three modules are stated below.

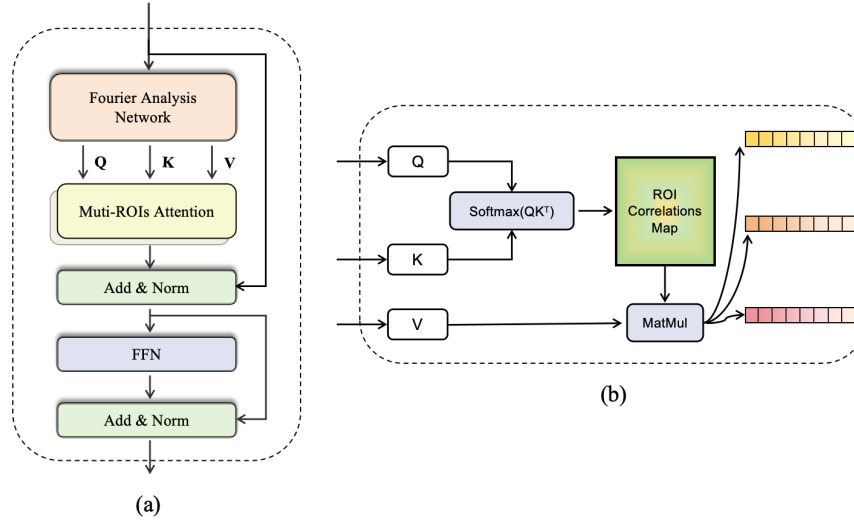


Fig. 3: (a) Illustration of SIAformer, in which self-attention (b) is applied to learning spatial interactions between ROIs.

B. Spatial Interaction Awareness

The conventional Transformer-based time series forecasters, such as Informer [17] and Autoformer [44], typically formed a (temporal) token by multiple variables of the same time point and performed the generative formulation of forecasting tasks. However, they may not be suitable for multivariate time series forecasting, particularly for the aforementioned fMRI time series forecasting task, due to the following reasons. First, fMRI data is unavoidably coupled with noise (which may be physiological, instrumental or motion-related) during image acquisition. This implies that a certain number of strong-noise tokens are mixed with all the tokens, and regarding all the tokens equally will potentially hinder the learning of true neural representations. Second, Transformer using the temporal tokens results in meaningless attention maps, and fails to capture multivariate correlations that are significant for characterizing between-ROI interactions in fMRI based brain network analysis.

Therefore, inspired by iTransformer [29], we design an SIA module (see Fig. 1(b)) to capture spatial dependencies between ROIs, i.e., multivariate correlations, where each univariate time series is embedded as a (variate) token, and the obtained variate tokens are implemented by our customized SIAformer for multivariate correlating and are individually input into a shared FFN for learning nonlinear representations. More specifically, we first embed each univariate time series in \mathbf{X}_P as a variate token of dimension D by a shared MLP, i.e.,

$$\mathbf{X}_E \in \mathbb{R}^{N \times D} := \text{Embedding}(\mathbf{X}_P). \quad (1)$$

The obtained variate tokens \mathbf{X}_E aggregate global information of time series over time, which can be better used by attention mechanisms in SIAformer for multivariate correlating below.

We subsequently use a stack of G SIAformer layers on \mathbf{X}_E , each composed of Fourier Analysis Network (FAN) [45], self-attention, and FFN, as shown in Fig. 3. More concretely, based on \mathbf{X}_E , FAN is employed to derive query, key, and value matrices ($\mathbf{Q}, \mathbf{K}, \mathbf{V} \in \mathbb{R}^{N \times D}$), i.e.,

$$(\mathbf{Q}, \mathbf{K}, \mathbf{V}) = \text{FAN}(\mathbf{X}_E), \quad (2)$$

respectively. The reason we use FAN here is that FAN can effectively extract implicit periodic patterns and regularities from the variate tokens through learnable spectral filters [46]. Based on the attention mechanism, we have the attention map matrix $\mathbf{A} \in \mathbb{R}^{N \times N}$ and token embedding matrix $\mathbf{H} \in \mathbb{R}^{N \times D}$ as

$$\mathbf{A} = \text{Softmax}\left(\frac{\mathbf{Q}\mathbf{K}^T}{\sqrt{D}}\right) \text{ and } \mathbf{H} = \mathbf{A}\mathbf{V}, \quad (3)$$

respectively. Of note, since each variate token corresponds to a specific ROI, the resulting attention map matrix \mathbf{A} can reflect the dependencies between ROIs. A shared FFN is applied to the embedding of each variate token in \mathbf{H} to further integrate relational information. In addition, as a basic operation widely used to enhance the convergence and training stability of deep neural networks, layer normalization (LN) is also performed. Finally, a comprehensive representation $\mathbf{H}^{\text{spat}} \in \mathbb{R}^{N \times D}$ that incorporates spatial interactions between ROIs is given by

$$\mathbf{H}^{\text{spat}} = \text{LN}(\text{FFN}(\mathbf{H}) + \text{LN}(\mathbf{H} + \mathbf{X}_E)), \quad (4)$$

which follows a gated or residual transformation.

C. Temporal Feature Refinement

To capture the temporal characteristics of fMRI time series, we present a TFR module using frequency domain techniques. Most frequency domain based time series forecasting methods tend to focus on high-energy components (low-frequency part) while ignoring low-energy components (high-frequency part), leading to sub-optimal prediction performance. Moreover, low-energy components of fMRI time series encode stable patterns of spontaneous neural activities [1], making them essential for fMRI time series forecasting. Therefore, we use Amplifier [47] as our TFR module (see Fig. 1(c)), because Amplifier can learn both low- and high-energy components without bias, as briefly stated in what follows.

We first equalize low- and high-energy components through spectrum flipping. Let $\mathcal{X}_P \in \mathbb{R}^{N \times L}$ denote the Discrete Fourier Transform (DFT) of \mathbf{X}_P , in which each row of \mathcal{X}_P is the

L -point DFT of the corresponding row of \mathbf{X}_P . Accordingly, the flipped spectrum satisfies, for $0 \leq k \leq L - 1$,

$$\mathcal{X}'_P[k] = \mathcal{X}_P[L - k]. \quad (5)$$

We apply the inverse DFT (IDFT) to the sum of \mathcal{X}'_P and \mathcal{X}_P , obtaining the energy-equalized time series $\mathbf{X}_P^{\text{eq}} \in \mathbb{R}^{N \times L}$, i.e.,

$$\mathbf{X}_P^{\text{eq}} = \text{IDFT}(\mathcal{X}_P + \mathcal{X}'_P). \quad (6)$$

As a result, the energy of the original low-energy components are increased to be commensurate with that of the high-energy components. The above energy equalization process is conducive to drawing the model's attention for learning the previously neglected low-energy components.

One can see from (6) that there will be two separate energy peaks at both ends of the spectrum of \mathbf{X}_P^{eq} . We subsequently adopt Seasonal-Trend Decomposition widely used in previous work [27], [44], [48] to decompose \mathbf{X}_P^{eq} into the seasonal and trend components as

$$\mathbf{X}_P^{\text{trend}}, \mathbf{X}_P^{\text{season}} = \text{Decom}(\mathbf{X}_P^{\text{eq}}), \quad (7)$$

which correspond to these two energy peaks. $\mathbf{X}_P^{\text{trend}}$ represents the slow, non-periodic modifications in fMRI time series, e.g., scanner drift or gradual physiological shift. In contrast, $\mathbf{X}_P^{\text{season}}$ delineates the periodic or cyclical patterns, reflecting experimental task repetitions or intrinsic physiological rhythms. Then, by applying two FFNs to the two peaks separately and fusing their outputs, we obtain $\mathbf{X}_P^{\text{ts}} \in \mathbb{R}^{N \times D}$ as

$$\mathbf{X}_P^{\text{ts}} = \text{FFN}_{\text{trend}}(\mathbf{X}_P^{\text{trend}}) + \text{FFN}_{\text{season}}(\mathbf{X}_P^{\text{season}}). \quad (8)$$

We finally adopt a linear transformation to adjust the column dimension of \mathbf{X}'_P to D (i.e., the column dimension of \mathbf{H}^{spat} in (4)), followed by an inverse operation of spectrum flipping to derive the temporal representation $\mathbf{H}^{\text{temp}} \in \mathbb{R}^{N \times D}$ (namely, the energy restoration process returns the energy to the original level), i.e.,

$$\begin{aligned} \hat{\mathbf{x}}'_P(n, :) &= \mathbf{X}'_P(n, :)\mathbf{W}_P + \mathbf{b}_P, \\ \mathbf{X}_P^{\text{ts}} &= \text{DFT}(\mathbf{X}_P^{\text{ts}}), \\ \mathbf{H}^{\text{temp}} &= \text{IDFT}(\mathbf{X}_P^{\text{ts}} - \hat{\mathbf{x}}'_P), \end{aligned} \quad (9)$$

where $\hat{\mathbf{x}}'_P(n, :)$ and $\mathbf{X}'_P(n, :)$ denote the n -th rows of $\hat{\mathbf{x}}'_P$ and \mathbf{X}'_P , respectively, $\mathbf{W}_P \in \mathbb{C}^{L \times D}$ is a complex-valued weight matrix, and $\mathbf{b}_P \in \mathbb{C}^D$ is a complex-valued bias vector.

D. Spatio-Temporal Pattern Alignment

The spatial and temporal representations (\mathbf{H}^{spat} and \mathbf{H}^{temp}) exhibit substantial differences in the high-level semantic representation space. Directly concatenating them can lead to redundancy and inconsistency. Therefore, based on vector similarity retrieval, we design an SPA module to align \mathbf{H}^{spat} with \mathbf{H}^{temp} , resulting in a global spatio-temporal representation, $\mathbf{H}^{\text{global}} \in \mathbb{R}^{N \times D}$, as illustrated in Fig. 1(d).

By three linear layers ψ_q, ψ_v , and ψ_k , we first project \mathbf{H}^{spat} and \mathbf{H}^{temp} to $\psi_q(\mathbf{H}^{\text{spat}})$, $\psi_k(\mathbf{H}^{\text{temp}})$, and $\psi_v(\mathbf{H}^{\text{temp}})$. Then, we compute the attention score matrix \mathbf{M} as

$$\mathbf{M} = \text{Softmax}(\psi_q(\mathbf{H}^{\text{spat}})(\psi_k(\mathbf{H}^{\text{temp}}))^{\top}), \quad (10)$$

and perform channel-wise feature aggregation by restoring channel dimension with the matrix multiplication of $\psi_v(\mathbf{H}^{\text{temp}})$ and \mathbf{M} . Finally, the output $\mathbf{H}^{\text{global}}$ is obtained as

$$\mathbf{H}^{\text{global}} = \omega(\psi_v(\mathbf{H}^{\text{temp}})\mathbf{M}) + \mathbf{H}^{\text{spat}}, \quad (11)$$

where ω stands for a linear layer. Via SPA, $\mathbf{H}^{\text{global}}$ explicitly captures both spatial and temporal dependencies among fMRI time series, enhancing the model's forecasting performance.

E. Forecasting Head and Loss Function

After extracting the latent representation $\mathbf{H}^{\text{global}}$, we employ a prediction head to transform the feature space into the target fMRI time series $\mathbf{X}_F \in \mathbb{R}^{N \times T}$, i.e., for $1 \leq n \leq N$,

$$\hat{\mathbf{X}}_F(n, :) = \mathbf{H}^{\text{global}}(n, :)\mathbf{W}_F + \mathbf{b}_F, \quad (12)$$

where $\mathbf{b}_F \in \mathbb{R}^T$ is a bias vector, and $\mathbf{W}_F \in \mathbb{R}^{D \times T}$ is a weight matrix. The model's parameters are optimized by minimizing the discrepancies between the predicted data $\hat{\mathbf{X}}_F$ in (12) and the ground-truth future data \mathbf{X}_F . For this purpose, we utilize the mean squared error (MSE) as the loss function; that is,

$$\mathcal{L}_{\text{MSE}} = \frac{1}{N} \sum_{n=1}^N \left\| \hat{\mathbf{X}}_F(n, :) - \mathbf{X}_F(n, :) \right\|_2^2. \quad (13)$$

TABLE I: Run duration and the number of frames (i.e., time points) per run for each fMRI paradigm.

fMRI paradigm	Frames per run	Run duration (min:sec)
Resting-state	1200	14:33
Working memory	405	5:01
Emotional processing	176	2:16
Language processing	316	3:57
Relational reasoning	232	2:56
Social cognition	274	3:27
Gambling	253	3:12
Motor execution	284	3:34

IV. EXPERIMENTAL RESULTS

A. Datasets and Preprocessing

In this study, we used the data from the Human Connectome Project (HCP) S1200 Release [24], which included behavioral and multi-modal neuroimaging datasets collected from 1206 healthy young adults aged 22 to 35 years. To ensure data integrity, a total of 862 subjects (409 males and 453 females) who had all four 3T MRI modalities (i.e., structural MRI, diffusion MRI, resting-state fMRI, and task fMRI) were selected. Detailed descriptions of their demographic characteristics and MRI acquisition parameters of the selected subjects can be readily found in the HCP protocol.

The resting-state fMRI data was acquired across two sessions (R1 and R2) on separate days, and we solely used the fMRI data at the first session (R1) in our study. The task fMRI data was acquired across seven task paradigms, including working memory, emotional processing, language processing, relational reasoning, social cognition, gambling, and motor execution. Two runs of the resting-state fMRI (R1) and each task fMRI

TABLE II: Performance comparison of different models on HCP-rs-fMRI and HCP-t-fMRI datasets. The mean is reported with the standard deviation shown in parentheses below. The best results are highlighted in bold.

Dataset	Metric	Model								
		Ours	iTransformer	DLinear	Amplifier	PatchTST	CrossFormer	FourierGNN	LSTM	RNN
HCP-rs-fMRI	MSE ↓	0.380 (0.004)	0.398 (0.002)	0.529 (0.012)	0.407 (0.006)	0.394 (0.003)	0.417 (0.001)	0.562 (0.005)	0.602 (0.013)	0.592 (0.006)
	MAE ↓	0.461 (0.004)	0.478 (0.002)	0.562 (0.009)	0.481 (0.005)	0.473 (0.004)	0.488 (0.003)	0.580 (0.004)	0.601 (0.011)	0.597 (0.008)
	R ↑	0.665 (0.002)	0.631 (0.001)	0.446 (0.013)	0.627 (0.006)	0.635 (0.003)	0.628 (0.004)	0.432 (0.002)	0.355 (0.008)	0.379 (0.005)
	R ² ↑	0.438 (0.003)	0.397 (0.003)	0.199 (0.011)	0.390 (0.003)	0.402 (0.005)	0.396 (0.006)	0.187 (0.003)	0.120 (0.007)	0.143 (0.007)
HCP-t-fMRI	MSE ↓	0.435 (0.004)	0.488 (0.004)	0.633 (0.005)	0.460 (0.009)	0.485 (0.006)	0.480 (0.010)	0.705 (0.007)	0.681 (0.005)	0.663 (0.004)
	MAE ↓	0.484 (0.006)	0.501 (0.002)	0.587 (0.007)	0.514 (0.015)	0.501 (0.003)	0.496 (0.008)	0.621 (0.005)	0.609 (0.010)	0.602 (0.008)
	R ↑	0.595 (0.003)	0.583 (0.005)	0.376 (0.004)	0.582 (0.021)	0.586 (0.005)	0.589 (0.017)	0.208 (0.009)	0.292 (0.007)	0.320 (0.008)
	R ² ↑	0.351 (0.004)	0.338 (0.002)	0.142 (0.003)	0.333 (0.018)	0.341 (0.008)	0.347 (0.013)	0.043 (0.004)	0.076 (0.002)	0.101 (0.004)

were implemented, one with a left-to-right and the other with a right-to-left phase encoding. To avoid the potential influence of the phase encoding direction on our study, we used the left-to-right phase encoding runs of all fMRI data. In Table I, we presented run duration and the number of time points (namely frames) per run for each fMRI paradigm.

All functional images underwent the HCP minimal preprocessing pipeline, including gradient distortion correction, head motion correction, image distortion correction, spatial alignment to standard Montreal Neurological Institute (MNI) space, and intensity normalization. Moreover, further denoising procedures were performed, which involved regressing out motion parameters (and their first-order derivatives), removal of linear trends, and temporal band-pass filtering (0.01–0.1 Hz). Afterwards, we parcellated all the preprocessed fMRI data into 268 (i.e., $N = 268$) ROIs based on the Shen functional atlas [49].

For simplicity, we denoted the above preprocessed resting-state fMRI data as HCP-rs-fMRI. We concatenated the preprocessed fMRI data from all the seven tasks along the temporal axis, and denoted the newly formed task fMRI data as HCP-t-fMRI. In this study, both HCP-rs-fMRI and HCP-t-fMRI were employed to evaluate the effectiveness of the proposed model for fMRI time series prediction, respectively.

B. Implementation Details

To avoid data leakage, we randomly split the whole subjects into 80% for training, 10% for validation, and 10% for testing, whose generative samples by sliding window were used as the training, validation, and test sets, respectively. This was repeated five times to reduce the influence of data-splitting bias, and the mean and standard deviation (std) of the prediction results in all test sets were reported on the four widely used evaluation metrics, including mean absolute error (MAE), mean squared error (MSE), Pearson’s correlation coefficient (R), and coefficient of determination (R²).

For parameter optimization, we selected the RMSprop optimizer, which adaptively adjusted the learning rate based on a moving average of squared gradients. The initial learning rate was set to 1×10^{-5} , and training was performed with a batch size of 64. To mitigate overfitting and improve generalization, an early stopping strategy was implemented, by which training was halted when the validation loss did not improve for 5 consecutive epochs. The main hyperparameters in our model were given as follows. The lengths of the previous and future fMRI time series over a sliding window were $L = 140$ and $T = 20$, respectively; and the stride was $s = 20$. Our model contained 2 SIAformer layers (namely $G = 2$) and 8 multi-head attention heads, and the embedding dimension was set to $D = 512$. Before feeding the time series data into our model, we normalized the data to stabilize training and improve robustness.

C. Forecasting Performance

With the use of HCP-rs-fMRI and HCP-t-fMRI, respectively, we compared the fMRI time series forecasting performance of our model (i.e., BrainCast) and 8 highly regarded baselines, including cutting-edge Transformer models (such as PatchTST [28], CrossFormer [18], and iTransformer [29]), efficient linear neural network models (such as DLinear [48] and Amplifier [47]), classic recurrent neural network models (such as LSTM [14] and RNN [15]), and graph neural network models (such as FourierGNN [30]).

As exhibited in Table II, BrainCast consistently achieved the best forecasting performance on these two datasets in terms of both the error-based metrics (MSE and MAE) and correlation-based metrics (R and R²). For example, on HCP-rs-fMRI, our model reached superior performance across all the metrics, decreasing MSE by ≥ 0.014 and MAE by ≥ 0.012 , and increasing R by ≥ 0.030 and R² by ≥ 0.036 . Similarly, on HCP-t-fMRI, our model outperformed the the second-best models by an obvious margin. Moreover, one can see that the Transformer models (also including ours) achieved better performance than

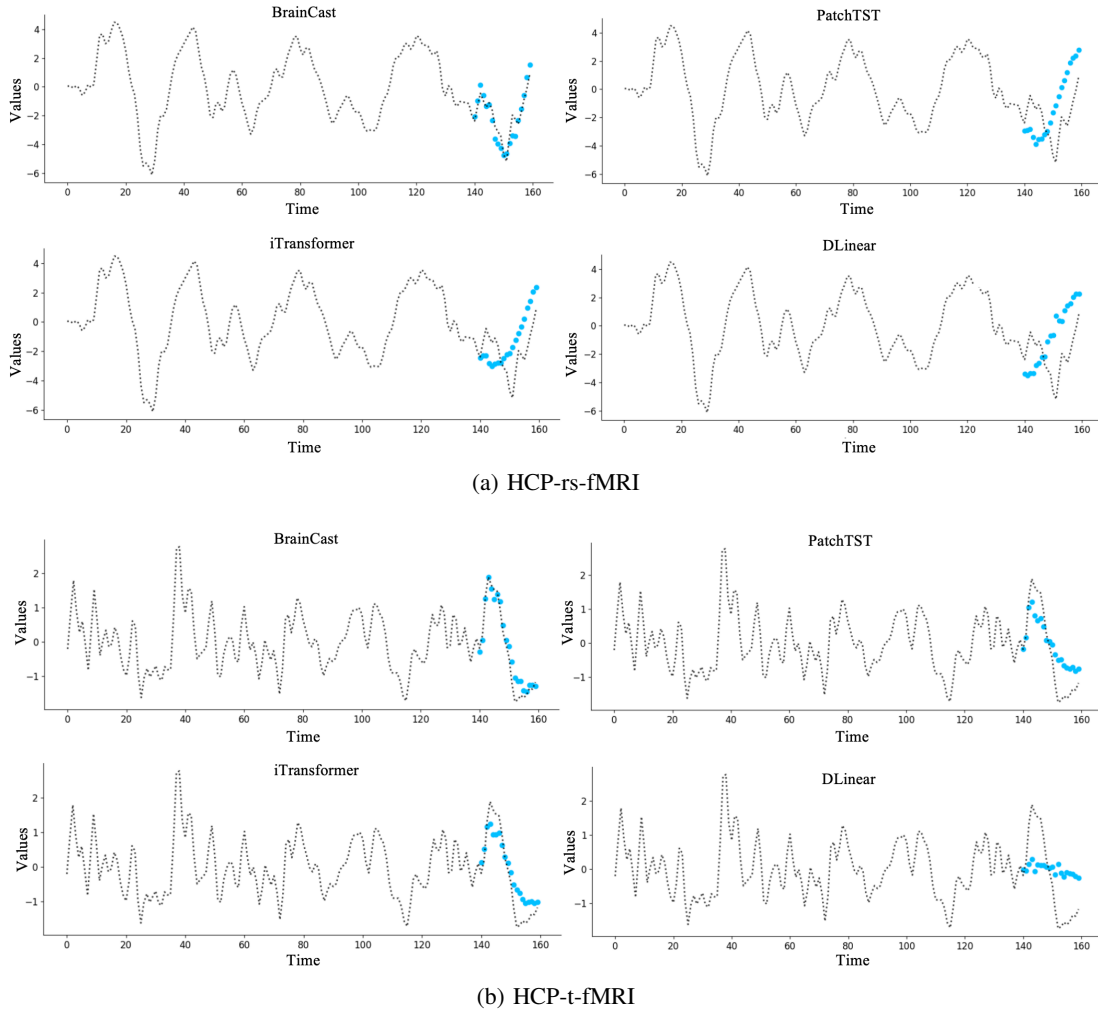


Fig. 4: Visualization of forecasting results on a randomly selected ROI of one test sample for HCP-rs-fMRI (a) and HCP-t-fMRI (b), respectively. The black dots denote the previous and ground-truth future data, and the blue dots denote the predicted data.

the others. In particular, such recurrent neural network architectures, i.e., LSTM and RNN, struggled to capture long-range dependencies in time series forecasting, leading to inferior performance. Although FourierGNN incorporated spectral representations of time series, its performance is limited in the fMRI time series forecasting tasks. This may be attributed to the complex spatio-temporal dynamics of brain neural activities that cannot be satisfactorily captured by frequency-domain analysis alone. By contrast, our model can practically characterize not only spatial interactions between ROIs but temporal variations within every ROI, highlighting its potential in modeling neural dynamics in multi-region fMRI time series.

To further demonstrate the superiority of our model, we visualized the forecasting results of our model, PatchTST, iTransformer, and DLinear in Fig. 4. For easy visualization, we presented the forecasting result of a randomly selected ROI of one test sample with respect to HCP-rs-fMRI and HCP-t-fMRI, respectively. As exhibited in Fig. 4, our model provided the most accurate predictions on future fMRI time series, substantially outperforming the other models, where the predicted trajectories not only followed the overall trend of the ground truth but

also aligned well with local fluctuations, including rising and falling patterns. In addition, we observed that despite the presence of rapid transitions or high-frequency oscillations in the time series, our model maintained stable forecasting accuracy. It indicates that our model is capable of learning both low-frequency trends and high-frequency variations in neural activity, which are essential to accurately modeling brain dynamics.

D. Ablation Studies

To verify whether the SIA, TFR, and SPA modules designed in our model were essential, we conducted ablation experiments on both HCP-rs-fMRI and HCP-t-fMRI, as shown in Fig. 5. One can see that removing any module consistently caused forecasting performance degradation across all evaluation metrics on both datasets. Specifically, removing TFR resulted in the most inferior performance, with MSE and MAE increasing while R and R^2 decreasing dramatically. This demonstrates the importance of modeling temporal dynamics for accurate fMRI time series forecasting. In addition, removing SIA also brought about significant performance decline, highlighting the necessity of capturing long-range spatial interactions between ROIs.

In comparison, SPA exerted a relatively small yet stable impact on performance, substantiating its vital role in aligning spatio-temporal representations output from SIA and TFR. Therefore, all such modules contributed to BrainCast in a complementary manner, and the full model achieved the best performance.

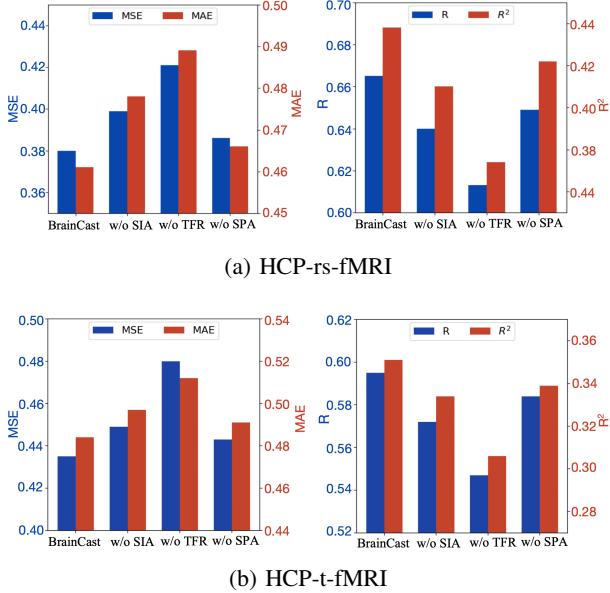


Fig. 5: Ablation results for the SIA, TFR, and SPA modules in our BrainCast on both HCP-rs-fMRI (a) and HCP-t-fMRI (b), respectively. The dark blue bars correspond to the left y-axis, whereas the dark red bars correspond to the right y-axis.

V. DISCUSSIONS

A. Visualization of Attention Maps

To elucidate the neurobiological underpinnings of our model for fMRI time series forecasting with HCP-rs-fMRI and HCP-t-fMRI, we visualized the cortical attention maps (i.e., the attention score matrices in (10)), respectively, by mapping the attention scores to the corresponding ROIs on the cortical surface; see Fig. 6. Notably, the attention map from HCP-rs-fMRI revealed pronounced left–right hemispheric symmetry, with conspicuous emphasis on homotopic regions, while that from HCP-t-fMRI lacked such symmetry and displayed a heterogeneous distribution of activated areas.

This striking bilateral symmetry during rest aligns well with prior findings on homotopic functional connectivity: the voxel-mirrored homotopic connectivity metric provides a quantitative measure of robust interhemispheric synchronization in regions, including cingulate, precentral, and postcentral gyri, therefore characterizing the intrinsic functional integration of homotopic areas at rest [50]. By contrast, task-driven states may attenuate this symmetric pattern of reliance. Task engagement typically recruits network-specific and lateralized circuits tailored to stimulus demands, consequently reducing the prominence of homotopic correspondence in predictive contributions. Actually, dynamic reconfiguration of resting-state networks—especially the default mode and dorsal attention subnetworks—has been demonstrated, with rest promoting bilateral coherence whereas

attention states elicit more lateralized, task-specific connectivity patterns [51].

Together, these observations suggest that during rest, homotopic connectivity provides a stable, symmetric scaffold exploited by the model for prediction, potentially reflecting underlying interhemispheric pathways. Under naturalistic stimulation, however, brain dynamics appear to become asymmetric, context-sensitive, attenuating the relative contribution of mirror regions and favoring specialized processing.

B. Influence of Look-Back Length

To investigate the impact of the length of the previous fMRI time series (i.e., L , also called look-back length) in BrainCast on the forecasting performance, we conducted additional experiments with varying $L \in \{100, 120, 140, 160, 180\}$ and fixed future length $T = 20$ (i.e., the length of the future fMRI time series) on both HCP-rs-fMRI and HCP-t-fMRI. As shown in Fig. 7, the fMRI time series forecasting performance measured by R initially improves with increasing L , achieves a peak at an intermediate value of $L = 140$, and then gradually declines as L continues to increase. This trend suggests a trade-off between contextual sufficiency and information redundancy. Increasing the look-back length initially enhances temporal modeling by providing richer historical context; however, when the look-back length becomes excessively long, the forecasting performance degrades as the model struggles to effectively capture increasingly complex temporal variations in extended sequences, and informative patterns might be diluted by redundant information. Conversely, overly short look-back lengths afford insufficient contextual information, limiting the model’s ability to characterize temporal dependencies and thereby impairing forecasting accuracy.

C. Application in Establishing Brain-Cognition Relationships

To explore the potential application of fMRI time series forecasting and evaluate the added value with BrainCast, we implemented designed experiments to investigate brain–cognition relationships. Specifically, we used two types of data (i.e., the previous fMRI time series and the prolonged fMRI time series extended by BrainCast) to predict the Penn Matrix Reasoning Test (PMAT) scores. As part of the HCP [24], the PMAT was carried out in the computerized neurocognitive battery (CNB) to quantify nonverbal reasoning-related cognitive ability [52]. In this setting, the previous fMRI time series of length 140 were augmented to the corresponding prolonged ones of length 160, with the last 20-point fMRI time series being forecasted by BrainCast. For the PMAT score prediction, we compared the root mean squared error (RMSE) derived from the previous and prolonged fMRI time series across a broad range of regression approaches, including convolutional neural networks (e.g., BrainNetCNN [33]), graph convolutional networks (e.g., GCN [37]), MLP [53], and support vector regression (SVR) [54], as reported in Table III. One can readily see that compared with the previous fMRI time series, the prolonged fMRI time series consistently improved the cognitive prediction performance across all the regression approaches. This finding underscores the potential applicability and impact of fMRI time series forecasting on neuroscience and clinical research.

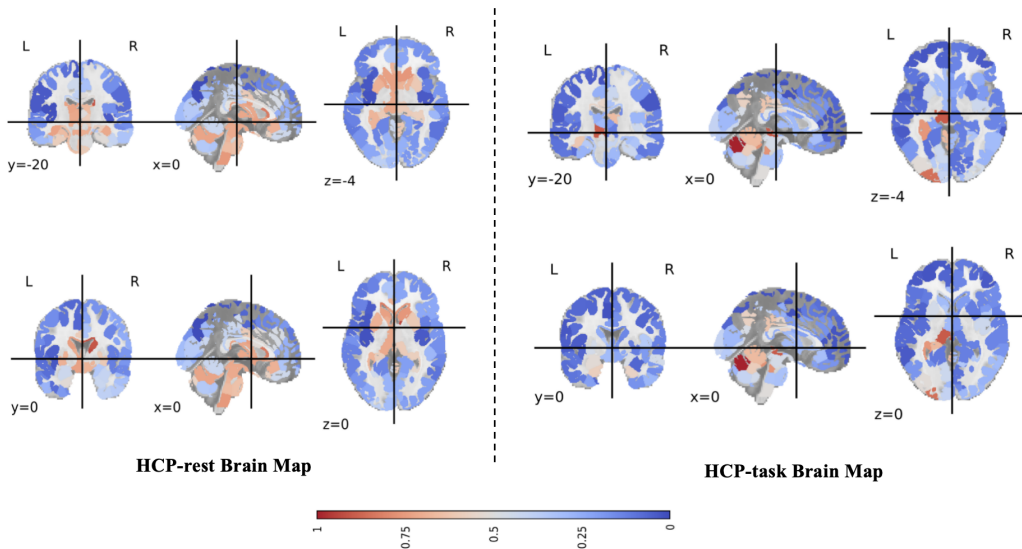


Fig. 6: Visualization of the cortical attention maps in the coronal, sagittal, and axial planes, where red indicates higher attention scores (i.e., greater contribution to the model’s prediction) and blue indicates lower contributions.

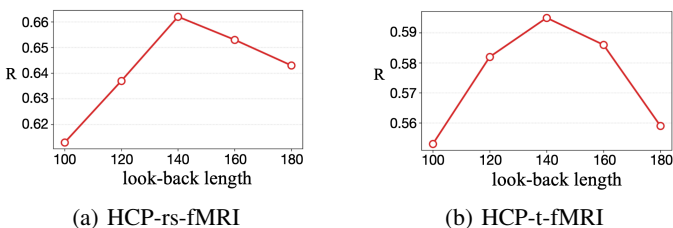


Fig. 7: The R results of BrainCast with varying look-back lengths (i.e., the length of the previous fMRI time series L) and the fixed future length (i.e., the length of the future fMRI time series $T = 20$) on both HCP-rs-fMRI and HCP-t-fMRI.

TABLE III: PMAT prediction performance on HCP-rs-fMRI, measured in terms of RMSE (mean \pm standard deviation).

Method	HCP-rs-fMRI (previous)	HCP-rs-fMRI (prolonged)
BrainNetCNN	5.0155 \pm 0.0017	4.8925 \pm 0.0303
MLP	4.8778 \pm 0.0382	4.7443 \pm 0.0221
GCN	4.8473 \pm 0.0150	4.7383 \pm 0.0470
SVR	4.7698 \pm 0.0121	4.6361 \pm 0.0598

VI. CONCLUSION

In this paper, we proposed BrainCast, a new spatio-temporal alignment driven framework for whole-brain fMRI time series forecasting. Through integrating the SIA, TFR, and SPA modules, our BrainCast can jointly capture inter-ROI spatial dependencies and intra-ROI temporal dynamics in a complementary and principled manner. Extensive experiments on both HCP-rs-fMRI and HCP-t-fMRI demonstrated that BrainCast consistently outperformed state-of-the-art time series forecasting models across several performance evaluation metrics. In addition, by augmenting the previous fMRI time series using BrainCast, we observed consistent improvements in downstream cognitive ability prediction. These results highlight the potential applica-

bility and added value of fMRI time series forecasting, which contributes to enhancing brain–cognition analyses, particularly in settings with limited scan durations. Future work will focus on subject-specific variability, multi-modal data fusion, and the clinical validation of BrainCast in neurological applications.

REFERENCES

- [1] M. D. Fox and M. E. Raichle, “Spontaneous fluctuations in brain activity observed with functional magnetic resonance imaging,” *Nature Reviews Neuroscience*, vol. 8, no. 9, pp. 700–711, 2007.
- [2] R. L. Buckner, J. R. Andrews-Hanna, and D. L. Schacter, “The brain’s default network: Anatomy, function, and relevance to disease,” *Annals of the New York Academy of Sciences*, vol. 1124, no. 1, pp. 1–38, 2008.
- [3] N. K. Logothetis, J. Pauls, M. Augath, T. Trinath, and A. Oeltermann, “Neurophysiological investigation of the basis of the fmri signal,” *Nature*, vol. 412, no. 6843, pp. 150–157, 2001.
- [4] N. K. Logothetis, “What we can do and what we cannot do with fmri,” *Nature*, vol. 453, no. 7197, pp. 869–878, 2008.
- [5] N. Schuff, N. Woerner, L. Boreta, T. Kornfield, L. Shaw, J. Trojanowski, P. Thompson, C. Jack Jr, M. Weiner, and A. D. N. Initiative, “Mri of hippocampal volume loss in early alzheimer’s disease in relation to apoe genotype and biomarkers,” *Brain*, vol. 132, no. 4, pp. 1067–1077, 2009.
- [6] P. Chen and T. Hemmen, “Evolving healthcare delivery in neurology during the coronavirus disease 2019 (covid-19) pandemic. *front neuro* 11: 578,” 2020.
- [7] K. Murphy, J. Bodurka, and P. A. Bandettini, “How long to scan? the relationship between fmri temporal signal to noise ratio and necessary scan duration,” *Neuroimage*, vol. 34, no. 2, pp. 565–574, 2007.
- [8] M. Pannunzi, R. Hindriks, R. G. Bettinardi, E. Wenger, N. Lisofsky, J. Martensson, O. Butler, E. Filevich, M. Becker, M. Lochstet *et al.*, “Resting-state fmri correlations: From link-wise unreliability to whole brain stability,” *Neuroimage*, vol. 157, pp. 250–262, 2017.
- [9] J. A. Nielsen, B. A. Zielinski, P. T. Fletcher, A. L. Alexander, N. Lange, E. D. Bigler, J. E. Lainhart, and J. S. Anderson, “Multisite functional connectivity mri classification of autism: Abide results,” *Frontiers in Human Neuroscience*, vol. 7, p. 599, 2013.
- [10] T. White, R. Muetzel, M. Schmidt, S. J. Langeslag, V. Jaddoe, A. Hofman, V. D. Calhoun, F. C. Verhulst, and H. Tiemeier, “Time of acquisition and network stability in pediatric resting-state functional magnetic resonance imaging,” *Brain Connectivity*, vol. 4, no. 6, pp. 417–427, 2014.
- [11] L. Q. R. Ooi, C. Orban, S. Zhang, T. E. Nichols, T. W. K. Tan, R. Kong, S. Marek, N. U. Dosenbach, T. O. Laumann, E. M. Gordon *et al.*, “Longer scans boost prediction and cut costs in brain-wide association studies,” *Nature*, vol. 644, no. 8077, pp. 731–740, 2025.

- [12] F. Sobczak, Y. He, T. J. Sejnowski, and X. Yu, "Predicting the fmri signal fluctuation with recurrent neural networks trained on vascular network dynamics," *Cerebral Cortex*, vol. 31, no. 2, pp. 826–844, 2021.
- [13] R. D. Hjelm, E. Damaraju, K. Cho, H. Laufs, S. M. Plis, and V. D. Calhoun, "Spatio-temporal dynamics of intrinsic networks in functional magnetic imaging data using recurrent neural networks," *Frontiers in Neuroscience*, vol. 12, p. 600, 2018.
- [14] T. Fischer and C. Krauss, "Deep learning with long short-term memory networks for financial market predictions," *European Journal of Operational Research*, vol. 270, no. 2, pp. 654–669, 2018.
- [15] Z. C. Lipton, J. Berkowitz, and C. Elkan, "A critical review of recurrent neural networks for sequence learning," *arXiv preprint arXiv:1506.00019*, 2015.
- [16] A. Vaswani, N. Shazeer, N. Parmar, J. Uszkoreit, L. Jones, A. N. Gomez, E. Kaiser, and I. Polosukhin, "Attention is all you need," *Advances in Neural Information Processing Systems*, vol. 30, 2017.
- [17] H. Zhou, S. Zhang, J. Peng, S. Zhang, J. Li, H. Xiong, and W. Zhang, "Informer: Beyond efficient transformer for long sequence time-series forecasting," in *Proceedings of the AAAI Conference on Artificial Intelligence*, vol. 35, no. 12, 2021, pp. 11 106–11 115.
- [18] Y. Zhang and J. Yan, "Crossformer: Transformer utilizing cross-dimension dependency for multivariate time series forecasting," in *The Eleventh International Conference on Learning Representations, 2023*.
- [19] J. O. Caro, A. H. d. O. Fonseca, C. Averill, S. A. Rizvi, M. Rosati, J. L. Cross, P. Mittal, E. Zappala, D. Levine, R. M. Dhodapkar *et al.*, "Brainlm: A foundation model for brain activity recordings," *bioRxiv*, pp. 2023–09, 2023.
- [20] W. Zheng, C. Bao, R. Mu, J. Wang, T. Li, Z. Zhao, Z. Yao, and B. Hu, "Frequency-specific dual-attention based adversarial network for blood oxygen level-dependent time series prediction," *Human Brain Mapping*, vol. 45, no. 14, p. e70032, 2024.
- [21] X. Li, Y. Zhou, N. Dvornek, M. Zhang, S. Gao, J. Zhuang, D. Scheinost, L. H. Staib, P. Ventola, and J. S. Duncan, "Braingnn: Interpretable brain graph neural network for fmri analysis," *Medical Image Analysis*, vol. 74, p. 102233, 2021.
- [22] X. Kan, W. Dai, H. Cui, Z. Zhang, Y. Guo, and C. Yang, "Brain network transformer," *Advances in Neural Information Processing Systems*, vol. 35, pp. 25 586–25 599, 2022.
- [23] Y. Yang, C. Ye, G. Su, Z. Zhang, Z. Chang, H. Chen, P. Chan, Y. Yu, and T. Ma, "Brainmass: Advancing brain network analysis for diagnosis with large-scale self-supervised learning," *IEEE Transactions on Medical Imaging*, vol. 43, no. 11, pp. 4004–4016, 2024.
- [24] D. C. Van Essen, K. Ugurbil, E. Auerbach, D. Barch, T. E. Behrens, R. Bucholz, A. Chang, L. Chen, M. Corbetta, S. W. Curtiss *et al.*, "The human connectome project: A data acquisition perspective," *Neuroimage*, vol. 62, no. 4, pp. 2222–2231, 2012.
- [25] C. Lea, M. D. Flynn, R. Vidal, A. Reiter, and G. D. Hager, "Temporal convolutional networks for action segmentation and detection," in *Proceedings of the IEEE Conference on Computer Vision and Pattern Recognition*, 2017, pp. 156–165.
- [26] H. Zhou, S. Zhang, J. Peng, S. Zhang, J. Li, H. Xiong, and W. Zhang, "Informer: Beyond efficient transformer for long sequence time-series forecasting," in *Proceedings of the AAAI conference on Artificial Intelligence*, vol. 35, no. 12, 2021, pp. 11 106–11 115.
- [27] T. Zhou, Z. Ma, Q. Wen, X. Wang, L. Sun, and R. Jin, "Fedformer: Frequency enhanced decomposed transformer for long-term series forecasting," in *International Conference on Machine Learning*. PMLR, 2022, pp. 27 268–27 286.
- [28] Y. Nie, N. H. Nguyen, P. Sinthong, and J. Kalagnanam, "A time series is worth 64 words: Long-term forecasting with transformers. arxiv 2022," *arXiv preprint arXiv:2211.14730*, 2022.
- [29] Y. Liu, T. Hu, H. Zhang, H. Wu, S. Wang, L. Ma, and M. Long, "Itrnformer: Inverted transformers are effective for time series forecasting," *arXiv preprint arXiv:2310.06625*, 2023.
- [30] K. Yi, Q. Zhang, W. Fan, H. He, L. Hu, P. Wang, N. An, L. Cao, and Z. Niu, "Fouriergnn: Rethinking multivariate time series forecasting from a pure graph perspective," *Advances in Neural Information Processing Systems*, vol. 36, pp. 69 638–69 660, 2023.
- [31] H. Han, M. Zhang, M. Hou, F. Zhang, Z. Wang, E. Chen, H. Wang, J. Ma, and Q. Liu, "Stgcn: A spatial-temporal aware graph learning method for poi recommendation," in *2020 IEEE International Conference on Data Mining (ICDM)*. IEEE, 2020, pp. 1052–1057.
- [32] Y. LeCun, Y. Bengio, and G. Hinton, "Deep learning," *Nature*, vol. 521, no. 7553, pp. 436–444, 2015.
- [33] J. Kawahara, C. J. Brown, S. P. Miller, B. G. Booth, V. Chau, R. E. Grunau, J. G. Zwicker, and G. Hamarneh, "Brainnetcn: Convolutional neural networks for brain networks; towards predicting neurodevelopment," *NeuroImage*, vol. 146, pp. 1038–1049, 2017.
- [34] H. Huang, X. Hu, Y. Zhao, M. Makkie, Q. Dong, S. Zhao, L. Guo, and T. Liu, "Modeling task fmri data via deep convolutional autoencoder," *IEEE Transactions on Medical Imaging*, vol. 37, no. 7, pp. 1551–1561, 2017.
- [35] B. Jie, M. Liu, C. Lian, F. Shi, and D. Shen, "Designing weighted correlation kernels in convolutional neural networks for functional connectivity based brain disease diagnosis," *Medical Image Analysis*, vol. 63, p. 101709, 2020.
- [36] F. Scarselli, M. Gori, A. C. Tsoi, M. Hagenbuchner, and G. Monfardini, "The graph neural network model," *IEEE Transactions on Neural Networks*, vol. 20, no. 1, pp. 61–80, 2008.
- [37] B. Jiang, Z. Zhang, D. Lin, J. Tang, and B. Luo, "Semi-supervised learning with graph learning-convolutional networks," in *Proceedings of the IEEE/CVF Conference on Computer Vision and Pattern Recognition*, 2019, pp. 11 313–11 320.
- [38] P. Velickovic, G. Cucurull, A. Casanova, A. Romero, P. Lio, Y. Bengio *et al.*, "Graph attention networks," *stat*, vol. 1050, no. 20, pp. 10–48 550, 2017.
- [39] X. Li, Y. Zhou, N. Dvornek, M. Zhang, S. Gao, J. Zhuang, D. Scheinost, L. H. Staib, P. Ventola, and J. S. Duncan, "Braingnn: Interpretable brain graph neural network for fmri analysis," *Medical Image Analysis*, vol. 74, p. 102233, 2021.
- [40] K. Zhao, B. Duka, H. Xie, D. J. Oathes, V. Calhoun, and Y. Zhang, "A dynamic graph convolutional neural network framework reveals new insights into connectome dysfunctions in adhd," *NeuroImage*, vol. 246, p. 118774, 2022.
- [41] C. Ying, T. Cai, S. Luo, S. Zheng, G. Ke, D. He, Y. Shen, and T.-Y. Liu, "Do transformers really perform badly for graph representation?" *Advances in Neural Information Processing Systems*, vol. 34, pp. 28 877–28 888, 2021.
- [42] D. Kreuzer, D. Beaini, W. Hamilton, V. Létourneau, and P. Tossou, "Rethinking graph transformers with spectral attention," *Advances in Neural Information Processing Systems*, vol. 34, pp. 21 618–21 629, 2021.
- [43] X. Kan, W. Dai, H. Cui, Z. Zhang, Y. Guo, and C. Yang, "Brain network transformer," *Advances in Neural Information Processing Systems*, vol. 35, pp. 25 586–25 599, 2022.
- [44] H. Wu, J. Xu, J. Wang, and M. Long, "Autoformer: Decomposition transformers with auto-correlation for long-term series forecasting," *Advances in Neural Information Processing Systems*, vol. 34, pp. 22 419–22 430, 2021.
- [45] Y. Dong, G. Li, Y. Tao, X. Jiang, K. Zhang, J. Li, J. Deng, J. Su, J. Zhang, and J. Xu, "Fan: Fourier analysis networks," *arXiv preprint arXiv:2410.02675*, 2024.
- [46] J. E. Chen and G. H. Glover, "Bold fractional contribution to resting-state functional connectivity above 0.1 hz," *Neuroimage*, vol. 107, pp. 207–218, 2015.
- [47] J. Fei, K. Yi, W. Fan, Q. Zhang, and Z. Niu, "Amplifier: Bringing attention to neglected low-energy components in time series forecasting," in *Proceedings of the AAAI Conference on Artificial Intelligence*, vol. 39, no. 11, 2025, pp. 11 645–11 653.
- [48] A. Zeng, M. Chen, L. Zhang, and Q. Xu, "Are transformers effective for time series forecasting?" in *Proceedings of the AAAI Conference on Artificial Intelligence*, vol. 37, no. 9, 2023, pp. 11 121–11 128.
- [49] X. Shen, F. Tokoglu, X. Papademetris, and R. T. Constable, "Groupwise whole-brain parcellation from resting-state fmri data for network node identification," *Neuroimage*, vol. 82, pp. 403–415, 2013.
- [50] X.-N. Zuo, C. Kelly, A. Di Martino, M. Mennes, D. S. Margulies, S. Bangaru, R. Grzadzinski, A. C. Evans, Y.-F. Zang, F. X. Castellanos *et al.*, "Growing together and growing apart: regional and sex differences in the lifespan developmental trajectories of functional homotopy," *Journal of Neuroscience*, vol. 30, no. 45, pp. 15 034–15 043, 2010.
- [51] M. W. Cole, D. S. Bassett, J. D. Power, T. S. Braver, and S. E. Petersen, "Intrinsic and task-evoked network architectures of the human brain," *Neuron*, vol. 83, no. 1, pp. 238–251, 2014.
- [52] J. Raven, "The raven's progressive matrices: Change and stability over culture and time," *Cognitive Psychology*, vol. 41, no. 1, pp. 1–48, 2000.
- [53] M.-C. Popescu, V. E. Balas, L. Perescu-Popescu, and N. Mastorakis, "Multilayer perceptron and neural networks," *WSEAS Transactions on Circuits and Systems*, vol. 8, no. 7, pp. 579–588, 2009.
- [54] M. Awad, R. Khanna, M. Awad, and R. Khanna, "Support vector regression. efficient learning machines: Theories, concepts, and applications for engineers and system designers, 67-80," 2015.